A NOVEL SECTIONAL CONSTITUTIVE MODEL FOR BEAM-COLUMN ELEMENT

Y. S. Chen[1,2] – B. Wu[1,2*] – T. L. Pan[1,2]

[1] Key Lab of Structures Dynamic Behavior and Control (Harbin Institute of Technology), Ministry of Education, Harbin 150090, China
[2] School of Civil Engineering, Harbin Institute of Technology, Harbin 150090, China

ARTICLE INFO

***Article history*:**
Received: 25.10.2014.
Received in revised form: 01.12.2014.
Accepted: 15.12.2014.

Keywords:
Constitutive model
Yield surface
Axial force and bending moment coupling
Mixed hardening
Elastoplastic analysis

Abstract:

The constitutive models on sectional level can meet both computational accuracy and efficiency, and hence have great potential for nonlinear analyses of frame structures. However, currently available sectional constitutive models usually assume a constant axial force and therefore cannot account for axial force and bending moment coupling flexibly. In this paper, a sectional constitutive model is proposed in the framework of classical plastic theory. The proposed model features kinematic/isotropic hardening. It can well account for axial flexure interaction, and can be used to describe distributed plasticity along beam-column members in comparison with a plastic hinge model. The numerical simulations of a cantilever column and a steel frame structure showed that the proposed sectional constitutive model is more accurate than a plastic hinge model and more efficient than a fiber model.

1 Introduction

Constitutive models are the basis for elastoplastic analyses of structures and/or components. As for beam-column elements, there are three levels of constitutive models [1]: member level [2], sectional level and material level [3], as shown in Fig. 1. The constitutive models on member level such as moment-rotation relation are used for concentrated plasticity. The other two models can be used for distributed plasticity. Among them the constitutive models on sectional level can meet both computational accuracy and efficiency, and thus are extensively studied [4-6]. However, the current sectional model is usually specified by a moment-curvature relation with fixed axial force, and it cannot account for axial force and bending moment coupling when the structural member is subject to varying axial force.

Yield surface of stress resultants offers a proper tool for considering axial and flexure interaction. A great research interest has been taken in such yield surface in the literature. Starting from the 1970s, Morris and Fenves [7], Nigam [8], Wen and Farhoomand [9] proposed a model for frame element that determines the elastoplastic state at the element ends using yield surface. Later in 1980s, Orbison [10] built a new yield surface for such a plastic hinge model, Powell and Chen [11] proposed a generalized plastic hinge model based on classical plastic theory. In 1990s, yield surface was employed in refined plastic hinge models [12], Shu and Shen

* Corresponding author. Tel.:+86-451-86283765 ; fax: +86-451-86282704
E-mail address: bin.wu@hit.edu.cn

[13] used yield surface for element ends state determination and verified it by a test. Chan and Chui [14] proposed a full plastic yield function for I and/or H cross-section and used it for plastic hinge elements. After 2000, yield surface has still been attractive. Iu et al. [15] employed a refined plastic hinge approach based on sectional yield surface to model the material non-linearity by strain-hardening of composite framed structures. Recent work using yield surface has been presented by Biglari et al. [16] for quasi-hinge beam element and Roncevic et al. [17] for establishing critical load of frame structures. However, in these plastic hinge models, the lumped plasticity assumption is not necessarily accurate [11], in quasi-hinge models, the length of the hinge which is specified by experience highly affects the simulation accuracy. Besides, some models even assume that plastic hinges only yield in bending with no inelastic axial deformation, which is not theoretically correct.

To account for axial force and bending moment coupling and to balance both computational accuracy and efficiency, a sectional constitutive model with mixed hardening is proposed in the framework of classical plastic theory. It can be used to describe distributed plasticity along beam-column members. The numerical implementation of the proposed model is introduced to determine the section state. Some numerical simulations are carried out to illustrate the accuracy and efficiency of the proposed model.

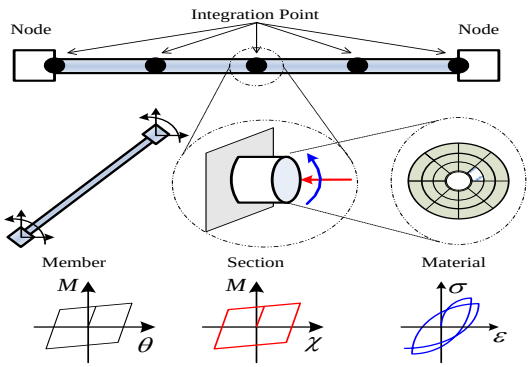

Figure 1. The three levels of restoring force model.

2 Sectional constitutive model with mixed hardening

The classical plastic theory is borrowed to derive the sectional constitutive model in this paper. We constrain discussion within the plane problem for simplicity, however, generalizing this case to three dimensions should not be a problem.

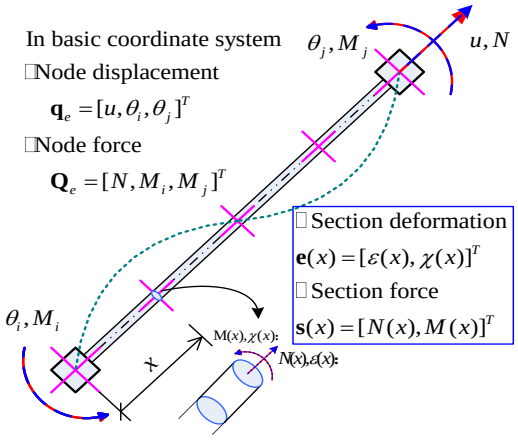

Figure 2. Forces and deformations at the element and section.

For a specified section in a beam-column element, see Fig. 2, let $\boldsymbol{e} = [\varepsilon_a, \chi]^T$ represent sectional deformation, in which ε_a and χ are axial deformation and curvature, respectively, and $\boldsymbol{s} = [N, M]^T$ represent sectional force, in which N and M are sectional axial force and bending moment, respectively. Then e and s are equivalent to the plane strain and stress of the classical plastic theory, respectively. To evaluate the sectional constitutive law, the assumptions are made as follows: (1) the plane section which initially has a normal to neutral axis remains plane and normal compared to the axis after deformation; (2) section yielding is defined as the state in which the stress at the whole cross-section attains yielding stress, and the state before such defined section yielding is assumed to be elastic, i.e., the transition from initial yielding to full yielding is neglected.

2.1 Sectional yield surface

Sectional yield surface specifies the yielding criterion of a section. There are plenty of literatures on construction of the yield surface considering axial force and moment interaction for different types of cross-sections [10, 14, 16, 18, 19], written by a lot of researchers, among them being Chan and Chui [14] who assumed that the inner area enclosing the center of the section takes the axial load and the remaining outer part resists the

moment to determine the yield surface of I or H section (see Fig. 3), and this concept is adopted herein. Therefore, yield surface can be obtained as:

$$\varphi(\mathbf{s})=\begin{cases}\dfrac{(2\alpha+1)^2}{4\alpha+1}\cdot\dfrac{N^2}{N_{\mathrm{y}}^2}+\dfrac{|M|}{M_{\mathrm{p}}}-1=0, & \dfrac{N}{N_{\mathrm{y}}}<\dfrac{1}{2\alpha+1}\\ \dfrac{|N|}{N_{\mathrm{y}}}+\dfrac{(4\alpha+1)}{2(2\alpha+1)}\cdot\dfrac{|M|}{M_{\mathrm{p}}}-1=0, & \dfrac{N}{N_{\mathrm{y}}}\geq\dfrac{1}{2\alpha+1}\end{cases}, \quad (1)$$

where $\varphi(\mathbf{s})$ is the sectional yield function, $\alpha=A_{\mathrm{f}}/A_{\mathrm{w}}$, in which A_{f} denotes the area of one flange, A_{w} denotes the area of web, and N_{y} is the axial yield force, M_{p} is the moment plastic strength in the absence of axial loads, they are expressed as:

$$\begin{aligned}N_{\mathrm{y}}&=Af_{\mathrm{y}}=(2\alpha+1)A_{\mathrm{w}}f_{\mathrm{y}}\\ M_{\mathrm{p}}&=W_{\mathrm{p}}f_{\mathrm{y}}=2A_{\mathrm{f}}f_{\mathrm{y}}d/2+2\times0.5A_{\mathrm{w}}f_{\mathrm{y}}d_{\mathrm{w}}/4\end{aligned}, \quad (2)$$

in which f_{y} is the yield stress of the material.

The above formulation does not account for hardening. For combined kinematic/isotropic hardening, Eq. (1) becomes:

$$\varphi(\mathbf{s},\boldsymbol{F}_{\mathrm{a}},\boldsymbol{F}_{\mathrm{y}})=\begin{cases}\dfrac{(2\alpha+1)^2}{4\alpha+1}\cdot\dfrac{(N-F_{\mathrm{a}N})^2}{F_{\mathrm{y}N}^2}+\dfrac{|M-F_{\mathrm{a}M}|}{F_{\mathrm{y}M}}-1=0, & \dfrac{N}{F_{\mathrm{y}N}}<\dfrac{1}{2\alpha+1}\\ \dfrac{|N-F_{\mathrm{a}N}|}{F_{\mathrm{y}N}}+\dfrac{(4\alpha+1)}{2(2\alpha+1)}\cdot\dfrac{|M-F_{\mathrm{a}M}|}{F_{\mathrm{y}M}}-1=0, & \dfrac{N}{F_{\mathrm{y}N}}\geq\dfrac{1}{2\alpha+1}\end{cases}, \quad (3)$$

where $\boldsymbol{F}_{\mathrm{a}}(\boldsymbol{e}^{\mathrm{p}})=(1-c)k_{\mathrm{h}}\boldsymbol{k}_{\mathrm{se}}\cdot\boldsymbol{e}^{\mathrm{p}}$ is a sectional back force vector, which contains two components, *i.e.*, $\boldsymbol{F}_{\mathrm{a}}=[F_{\mathrm{a}N},F_{\mathrm{a}M}]^T$. $\boldsymbol{F}_{\mathrm{y}}(\boldsymbol{e}^{\mathrm{p}})=\boldsymbol{F}_{\mathrm{y}0}+c\cdot i_{\mathrm{h}}\boldsymbol{k}_{\mathrm{se}}\cdot\left|\boldsymbol{e}^{\mathrm{p}}\right|$ denotes a sectional yield force vector, which contains two components, *i.e.*, $\boldsymbol{F}_{\mathrm{y}}=[F_{\mathrm{y}N},F_{\mathrm{y}M}]^T$; $\boldsymbol{e}^{\mathrm{p}}$ is a plastic deformation vector, $\boldsymbol{k}_{\mathrm{se}}$ is an elastic stiffness matrix, and k_{h} is a kinematic hardening coefficient, i_{h} is an isotropic hardening coefficient; $c\in[0,1]$; if c = 1, it is isotropic hardening, if c = 0, it is kinematic hardening, if $c\in(0,1)$, it is mixed hardening.

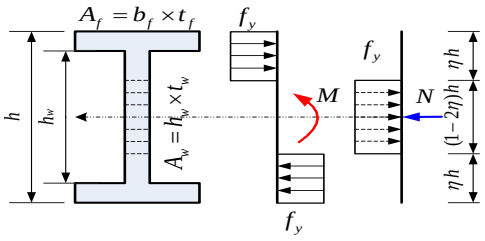

Figure 3. H-Section and internal force analysis.

2.2 Relation between sectional force and deformation

According to classical plasticity theory, the sectional generalized force results only from the elastic part of the deformation, and the relation is expressed in incremental form as:

$$\mathrm{d}\boldsymbol{s}=\boldsymbol{k}_{\mathrm{se}}\cdot(\mathrm{d}\boldsymbol{e}-\mathrm{d}\boldsymbol{e}^{\mathrm{p}}), \quad (4)$$

where $\boldsymbol{k}_{\mathrm{se}}=\begin{bmatrix}EA & 0\\ 0 & EI\end{bmatrix}$ is the elastic stiffness matrix at the specified section. E is the material elastic modulus, A is the area of the cross-section, and I is the moment of inertia of the cross-section.

According to Drucker postulate, when the material is in associative flow state, plastic deformation goes along the outward normal direction of yield surface.

$$\mathrm{d}\boldsymbol{e}^{\mathrm{p}}=\mathrm{d}\lambda\cdot\boldsymbol{G}, \quad (5)$$

where $\boldsymbol{G}=\partial\varphi/\partial\mathbf{s}$ is the outward normal direction of yield surface, and $\mathrm{d}\lambda$ is the magnitude of plastic deformation increment, which will be determined and discussed in 3.2.

The kinematic and isotropic hardening law is expressed in Eqs. (6) and (7). The back force increment in cross-section is proportional to the plastic deformation increment, and it can be written as:

$$\mathrm{d}\boldsymbol{F}_{\mathrm{a}}=k_{\mathrm{h}}\boldsymbol{k}_{\mathrm{se}}\cdot\mathrm{d}\boldsymbol{e}^{\mathrm{p}}. \quad (6)$$

The yield force increment of the cross-section is proportional to the absolute value of plastic deformation increment, and it can be expressed as:

$$\mathrm{d}\boldsymbol{F}_{\mathrm{y}}=i_{\mathrm{h}}\boldsymbol{k}_{\mathrm{se}}\cdot\left|\mathrm{d}\boldsymbol{e}^{\mathrm{p}}\right|. \quad (7)$$

To determine the path of sectional force, Kuhn-Tucher loading/unloading (complementarities) condition is used:

$$\mathrm{d}\lambda \cdot \varphi(\boldsymbol{s}, \boldsymbol{F}_{\mathrm{a}}, \boldsymbol{F}_{\mathrm{y}}) = 0 \quad . \tag{8}$$

3 Section state determination and constitutive relation integration

For a given integration section in distributed plasticity models [**Error! Bookmark not defined.**], the numerical implementation method for the proposed sectional constitutive model is mainly discussed with the help of the schematic of cross-section force space and force path, (see Fig. 4, where *M* denotes the sectional bending moment, while *N* denotes the sectional axial force).

3.1 Section state determination

In time incremental step or iterative step, when proceeding from *j*th step to $(j+1)$th step, the state determination of a specified section is to obtain the sectional force and update sectional stiffness matrix with the known information at *j*th step and section deformation at $(j+1)$th step from the analysis on the structural and element levels. The main steps of section state determination are listed as follows.

1) To compute the trial force. The predicted force increment $\Delta\tilde{\boldsymbol{s}}$ is calculated on elastic assumption, and the $(j+1)$th step trial force ${}^{j+1}\boldsymbol{s}^{\mathbf{trial}}$ is obtained by adding $\Delta\tilde{\boldsymbol{s}}$ to ${}^{j}\boldsymbol{s}$:

$$\Delta\tilde{\boldsymbol{s}} = \boldsymbol{k}_{\mathrm{se}} \cdot \Delta\boldsymbol{e}\,, \tag{9}$$

$${}^{j+1}\boldsymbol{s}^{\mathbf{trial}} = {}^{j}\boldsymbol{s} + \Delta\tilde{\boldsymbol{s}}\,. \tag{10}$$

2) To determine the section elastic/plastic state. Substituting the trial force ${}^{j+1}\boldsymbol{s}^{trial}$ into yield function $\varphi({}^{j+1}\boldsymbol{s}^{trial}, {}^{j}\boldsymbol{F}_{\mathrm{a}}, {}^{j}\boldsymbol{F}_{\mathrm{y}})$ of the section, the scale factor *r* (see Fig. 4) and the new state ${}^{j+1}State$ can be obtained from $\varphi({}^{j+1}\boldsymbol{s}^{trial}, {}^{j}\boldsymbol{F}_{\mathrm{a}}, {}^{j}\boldsymbol{F}_{\mathrm{y}})$ and ${}^{j}State$:

When ${}^{j}State$ =0, in other words, the last state of the section is elastic:

a) if $\varphi({}^{j+1}\boldsymbol{s}^{trial}, {}^{j}\boldsymbol{F}_{\mathrm{a}}, {}^{j}\boldsymbol{F}_{\mathrm{y}}) \prec 0$, then the current state is also elastic, let ${}^{j+1}State = 0$ and $r = 1$.

b) if $\varphi({}^{j+1}\boldsymbol{s}^{trial}, {}^{j}\boldsymbol{F}_{\mathrm{a}}, {}^{j}\boldsymbol{F}_{\mathrm{y}}) \geq 0$, the current state changes to plasticity, let ${}^{j+1}State$ =1 and compute the scale factor r.

When ${}^{j}State$ =1, in other words, the last state of the section is plastic:

a) if $\varphi({}^{j+1}\boldsymbol{s}^{trial}, {}^{j}\boldsymbol{F}_{\mathrm{a}}, {}^{j}\boldsymbol{F}_{\mathrm{y}}) \prec 0$, then the current state changes to elasticity, let ${}^{j+1}State = 0$ and $r = 1$.

b) if $\varphi({}^{j+1}\boldsymbol{s}^{trial}, {}^{j}\boldsymbol{F}_{\mathrm{a}}, {}^{j}\boldsymbol{F}_{\mathrm{y}}) \geq 0$ then the current state is also plastic, let ${}^{j+1}State = 1$ and $r = 0$.

3) To calculate force increment. Calculating the force increment $\Delta\boldsymbol{s}$ corresponding to deformation increment $\Delta\boldsymbol{e}$. The deformation increment $\Delta\boldsymbol{e}$ is divided into two parts, $r\cdot\Delta\boldsymbol{e}$ and $(1-r)\cdot\Delta\boldsymbol{e}$. The former results in a pure elastic response, while the latter results in an elastic-plastic one [20]. Hence, the force increment may be integrated as:

$$\Delta\boldsymbol{s} = \int_{{}^{j}\boldsymbol{e}}^{{}^{j}\boldsymbol{e}+\Delta\boldsymbol{e}} \boldsymbol{k}_{\mathrm{se}} \cdot (\mathrm{d}\boldsymbol{e} - \mathrm{d}\boldsymbol{e}^{\mathrm{p}}) = r\cdot\Delta\tilde{\boldsymbol{s}} + \int_{{}^{j}\boldsymbol{e}+r\Delta\boldsymbol{e}}^{{}^{j}\boldsymbol{e}+\Delta\boldsymbol{e}} \boldsymbol{k}_{\mathrm{se}} \cdot (\mathrm{d}\boldsymbol{e} - \mathrm{d}\boldsymbol{e}^{\mathrm{p}})$$

$$= \Delta\boldsymbol{s}_1 + \Delta\boldsymbol{s}_2\,, \tag{11}$$

where $\Delta\boldsymbol{s}_1 = r\cdot\Delta\tilde{\boldsymbol{s}}$ results from $r\cdot\Delta\boldsymbol{e}$,

$\Delta\boldsymbol{s}_2 = \int_{{}^{j}\boldsymbol{e}+r\Delta\boldsymbol{e}}^{{}^{j}\boldsymbol{e}+\Delta\boldsymbol{e}} \boldsymbol{k}_{\mathrm{se}} \cdot (\mathrm{d}\boldsymbol{e} - \mathrm{d}\boldsymbol{e}^{\mathrm{p}})$ results from $(1-r)\cdot\Delta\boldsymbol{e}$.

4) To update correlated quantities.

$${}^{j+1}\boldsymbol{s} = {}^{j}\boldsymbol{s} + \Delta\boldsymbol{s} \tag{12 a}$$

$${}^{j+1}\boldsymbol{e}^{\mathrm{p}} = {}^{j}\boldsymbol{e}^{\mathrm{p}} + \Delta\boldsymbol{e}^{\mathrm{p}} \tag{12 b}$$

$${}^{j+1}\boldsymbol{F}_{\mathrm{a}} = {}^{j}\boldsymbol{F}_{\mathrm{a}} + k_{\mathrm{h}}\boldsymbol{k}_{\mathrm{se}} \cdot \Delta\boldsymbol{e}^{\mathrm{p}} \tag{12 c}$$

$${}^{j+1}\boldsymbol{F}_{\mathrm{y}} = {}^{j}\boldsymbol{F}_{\mathrm{y}} + i_{\mathrm{h}}\boldsymbol{k}_{\mathrm{se}} \cdot \left|\Delta\boldsymbol{e}^{\mathrm{p}}\right| \tag{12 d}$$

Loop (9) to (12) step for each integration section.

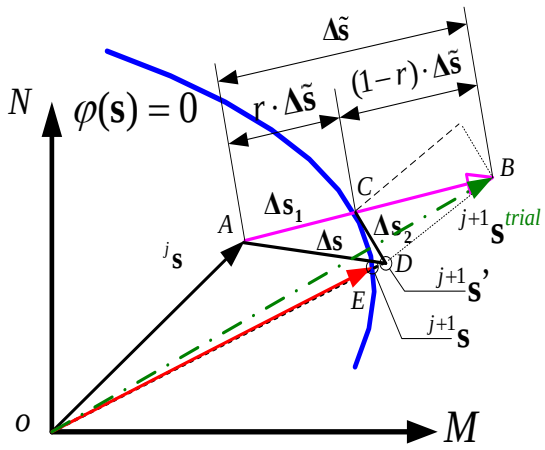

Figure 4. The schematic of yield surface and force path in force space.

3.2 Constitutive relation integration

Herein, the force increment $\Delta \boldsymbol{s}_2$ arising from $\Delta \boldsymbol{e}_2 = (1-r)\Delta \boldsymbol{e}$ is mainly discussed. The tangential prediction and radial return algorithm [21] based on explicit integration are used to solve Eq. (11).

1) Tangential prediction:

$$\Delta \boldsymbol{s}_2 = \int_{{}^{j}\boldsymbol{e}+r\Delta \boldsymbol{e}}^{{}^{j}\boldsymbol{e}+\Delta \boldsymbol{e}} \boldsymbol{k}_{\mathrm{se}} \cdot (\mathrm{d}\boldsymbol{e} - \mathrm{d}\boldsymbol{e}^{\mathrm{p}}) = \boldsymbol{k}_{\mathrm{se}} \cdot (\Delta \boldsymbol{e}_2 - \Delta \boldsymbol{e}_2^{\mathrm{p}}) \ , \quad (13)$$

where $\Delta \boldsymbol{e}_2^{\mathrm{p}}$ is the plastic deformation increment corresponding to $\Delta \boldsymbol{e}_2$.

Assuming the general yield surface of a section,

$$\varphi(\boldsymbol{s}, \boldsymbol{F}_{\mathrm{a}}, \boldsymbol{F}_{\mathrm{y}}) = 0 \ . \quad (14)$$

According to the consistency condition, the total differential form of the yield function [22] is:

$$\mathrm{d}\varphi = (\frac{\partial \varphi}{\partial \boldsymbol{s}})^{\mathrm{T}} \cdot \mathrm{d}\boldsymbol{s} + (\frac{\partial \varphi}{\partial \boldsymbol{F}_{\mathrm{a}}})^{\mathrm{T}} \cdot \mathrm{d}\boldsymbol{F}_a + (\frac{\partial \varphi}{\partial \boldsymbol{F}_{\mathrm{y}}})^{\mathrm{T}} \cdot \mathrm{d}\boldsymbol{F}_{\mathrm{y}} = 0 \ . \quad (15)$$

Substitute Eqs. (4-7) into Eq. 15:

$$\begin{aligned} &\mathrm{d}\varphi = \boldsymbol{G}^{\mathrm{T}} \cdot \boldsymbol{k}_{\mathrm{se}} \cdot (\mathrm{d}\boldsymbol{e} - d\lambda \cdot \boldsymbol{G}) + \\ &\mathrm{d}\lambda \cdot k_{\mathrm{h}} \cdot \boldsymbol{G}_1^{\mathrm{T}} \boldsymbol{k}_{\mathrm{se}} \boldsymbol{G} + \mathrm{d}\lambda \cdot i_{\mathrm{h}} \cdot \boldsymbol{G}_2^{\mathrm{T}} \boldsymbol{k}_{\mathrm{se}} \boldsymbol{G} = 0 \end{aligned} \ , \quad (16)$$

where $\boldsymbol{G}_1 = \partial \varphi / \partial \boldsymbol{F}_{\mathrm{a}}$, $\boldsymbol{G}_2 = \partial \varphi / \partial \boldsymbol{F}_{\mathrm{y}}$.

The scalar $\mathrm{d}\lambda$ which is the magnitude of plastic deformation increment may be expressed as:

$$\mathrm{d}\lambda = L / H \ , \quad (17)$$

where L is the loading criterion function defined as:

$$L = \boldsymbol{G}^{\mathrm{T}} \boldsymbol{k}_{se} \cdot \mathrm{d}\boldsymbol{e} \ , \quad (18a)$$

and H is a positive scalar that can be expressed as:

$$H = \boldsymbol{G}^{\mathrm{T}} \boldsymbol{k}_{\mathrm{se}} \boldsymbol{G} - k_{\mathrm{h}} \cdot \boldsymbol{G}_1^{\mathrm{T}} \boldsymbol{k}_{\mathrm{se}} \boldsymbol{G} - i_{\mathrm{h}} \cdot \boldsymbol{G}_2^{\mathrm{T}} \boldsymbol{k}_{\mathrm{se}} \boldsymbol{G} \ . \quad (18b)$$

Thus, the incremental form relation of sectional force and deformation at plastic stage is expressed as:

$$\mathrm{d}\boldsymbol{s} = (\boldsymbol{k}_{\mathrm{se}} - \boldsymbol{k}_{\mathrm{sp}}) \cdot \mathrm{d}\boldsymbol{e} = \boldsymbol{k}_{\mathrm{sep}} \cdot \mathrm{d}\boldsymbol{e} \ , \quad (19)$$

where $\boldsymbol{k}_{\mathrm{sp}} = (\boldsymbol{k}_{\mathrm{se}} \cdot \boldsymbol{G}\boldsymbol{G}^{\mathrm{T}} \cdot \boldsymbol{k}_{\mathrm{se}}) / H$ is sectional plastic stiffness matri, $\boldsymbol{k}_{\mathrm{sep}}$ is sectional elastoplastic stiffness matrix. Then Eq. (19) is changed into finite incremental form and written corresponding to Eq. (13):

$$\Delta \boldsymbol{s}_2 = (\boldsymbol{k}_{\mathrm{se}} - \boldsymbol{k}_{\mathrm{sp}}) \Delta \boldsymbol{e}_2 = \boldsymbol{k}_{\mathrm{sep}} \Delta \boldsymbol{e}_2 \ . \quad (20)$$

2) Radial return algorithm

In Eq. (20), the explicit Eulerian method is employed; $\boldsymbol{k}_{\mathrm{sep}}$ is the tangential stiffness of point C (see Fig. 4), thus, $\Delta \boldsymbol{s}_2$ is in the tangential direction of point C. Since the yield surface is outer convex, ${}^{j+1}\boldsymbol{s}'$ (point D) is always outside of the yield surface. In order to meet the consistent conditions, it is necessary to bring the force point to the yield surface, such as ${}^{j+1}\boldsymbol{s}$ (point E).

Such a correction is often achieved by adding a correction vector to the force vector in the direction normal to the yield surface.

$$\delta \mathbf{s} = a \cdot \boldsymbol{G} \ , \quad (21)$$

where a is a small scalar to be determined such that the yield condition is satisfied at the corrected force state:

$$\varphi({}^{j+1}\boldsymbol{s}' + \delta \boldsymbol{s}, \boldsymbol{F}_{\mathrm{a}}, \boldsymbol{F}_{\mathrm{y}}) = \varphi({}^{j+1}\boldsymbol{s}' + a \cdot \boldsymbol{G}, \boldsymbol{F}_{\mathrm{a}}, \boldsymbol{F}_{\mathrm{y}}) = 0 \ . \quad (22)$$

To solve the nonlinear equation of the scalar a, herein, the Taylor series expansion is used and all

higher-order terms than the linear ones are neglected, the scalar a is obtained as:

$$a = \frac{-\varphi(^{j+1}\boldsymbol{s}', \boldsymbol{F}_a, \boldsymbol{F}_y)}{\boldsymbol{G}^T\boldsymbol{G}}. \quad (23)$$

Finally, the corrected force vector can be expressed as:

$$^{j+1}\boldsymbol{s} = ^{j+1}\boldsymbol{s}' + a \cdot \boldsymbol{G}. \quad (24)$$

4 Numerical examples

Two numerical examples including a static cyclic analysis and a dynamic analysis are carried out to investigate the performance of the proposed sectional constitutive model with mixed hardening.

4.1 Static analysis

Taking H-section steel cantilever column as an example, the geometrical dimension and load information are shown in Fig. 5. The steel is Q 235 with yield stress of 235 MPa, and the section type is WH 250×250 [23]. The ratio of axial force to sectional yield force is 0.60. The lateral displacement loading history shown in Fig. 6 is applied at the top of the cantilever column.

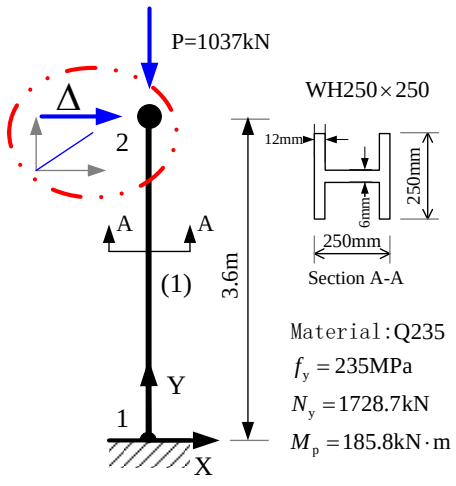

Figure 5. Static cycle analysis of a cantilever column.

Three models are considered: the first is the sectional constitutive model proposed in 2.2 of this paper denoted as Section, the second is fiber element denoted as Fiber, and the third is plastic hinge model denoted as Hinge. All these three cases are programmed with MATLAB [24] while the second case is also analyzed with OpenSEES [25] for comparison accuracy. The kinematic hardening coefficient k_h and isotropic-hardening coefficient i_h are both 3/97 for the sectional and fiber models.

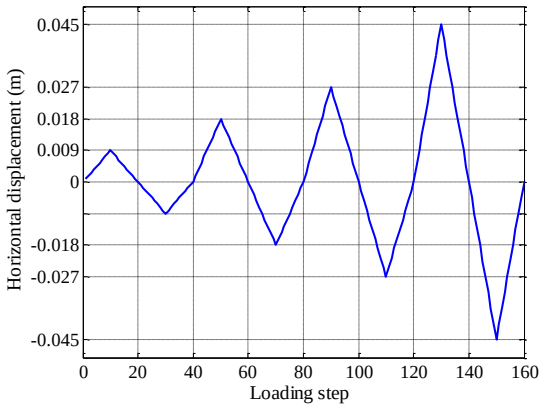

Figure 6. Horizontal displacement commands at the top node.

But only kinematic hardening is considered for the plastic hinge model which is composed of perfect-plastic hinge and elastic beam/column in parallel, and the equivalent kinematic hardening coefficient herein is also 3/97. For the fiber model, the section is divided into 14 patches, two for each flange and ten for the web. The flexibility formulation is employed on the element level for the analyses with sectional model and fiber model, and the Gauss-Lobatto integration algorithm is adopted with five integration sections. For the plastic hinge model, the plasticity is concentrated on the bottom of the column, and the rest of the column is assumed to be elastic. The Newton-Raphson algorithm is used for iteration of structural analysis and energy error tolerance is 10^{-6}.

The base shear force versus top horizontal displacement of the cantilever column is shown in Fig. 7. The moment-curvature relation of the bottom section is shown in Fig. 8. The internal force path and yield surface of the bottom section is shown in Fig. 9.

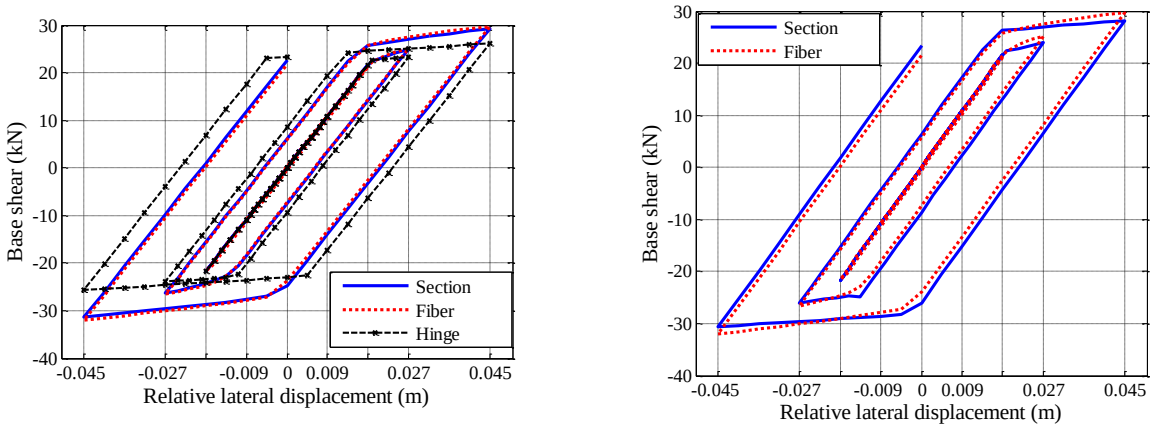

(a) Kinematic hardening *(b) Isotropic hardening*

Figure 7. Bottom shear force vs top horizontal displacement of the cantilever column.

It can be seen from Fig. 7 that the structural responses with proposed sectional model agree very well with those obtained with fiber model of OpenSEES. But the response obtained from plastic hinge with kinematic hardening is apparently different from those of the other two, which indicate that the accuracy of the proposed approach is much higher than the one achieved with the plastic hinge model.

From Figures 8 and 9, it can be observed that (1) the plastic bending moment capacity is reduced in the presence of axial force, indicating that the sectional model can well account for axial force and bending moment coupling; (2) with the accumulation of plastic deformation, yield surface moves with kinematic hardening and expands with isotropic hardening, indicating that the hardening is well handled with the proposed sectional model.

In Fig. 8, the moment-curvature relation at the bottom section of the cantilever obtained from the sectional model is a little different from that obtained from fiber model with OpenSEES. The reason is that the yield criteria employed in the two cases are different: the former adopts full section plasticity, while the latter corresponds to fiber yield. However, the difference exists only on section level, whereas the structural responses are nearly the same for the two models as seen in Fig. 7.

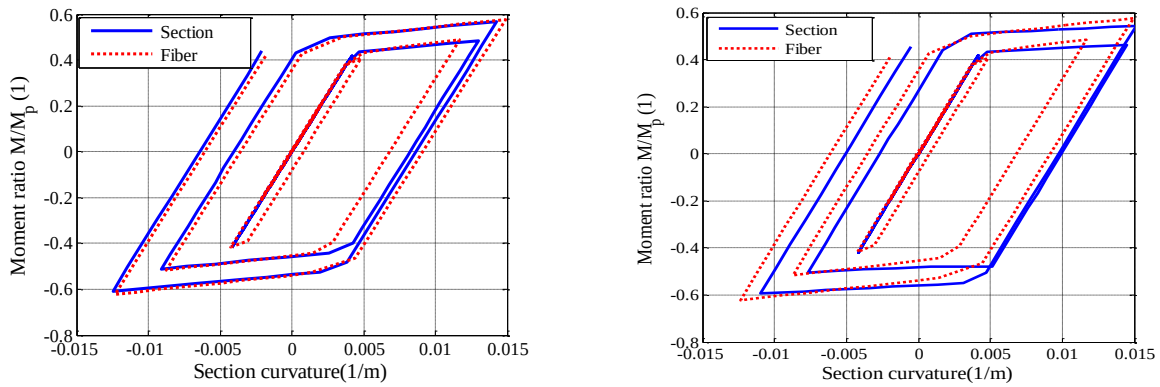

(a) Kinematic hardening *(b) Isotropic hardening*

Figure 8. Moment-curvature relation of the bottom section.

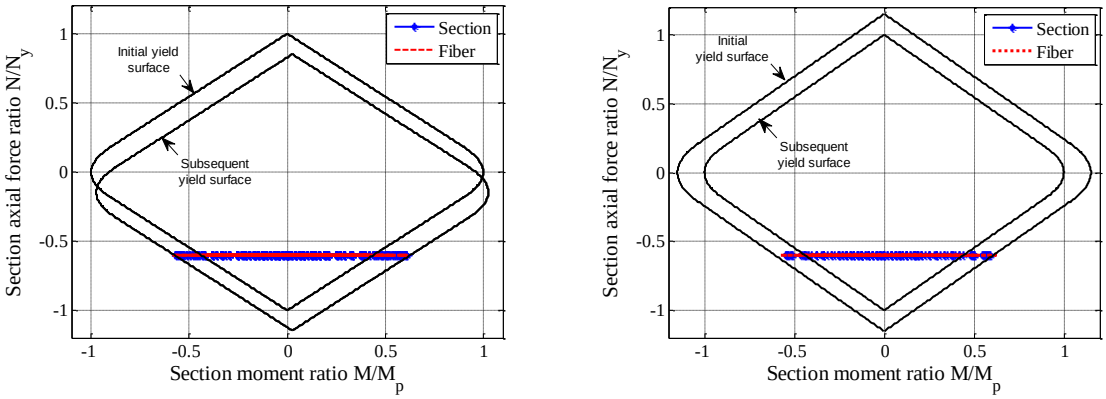

(a) Kinematic hardening *(b) Isotropic hardening*

Figure 9. Internal force path and yield surface of the bottom integration.

Table 1. Time consumption comparison of section model and fiber model

Cases	Section model, t_A (s)	Fiber model, t_B (s)	t_B / t_A
Kinematic Hardening	18.81	51.55 (MATLAB)	2.74
Isotropic Hardening	7.34	17.73 (MATLAB)	2.41
Cumputer: Pentium IV Processor, CPU 2.8 GHz, RAM 2.0 G.			

The time consumptions of the section and fiber models with programs both written in MATLAB are compared and the results are listed in Table 1. The computation is carried out using the same computer with Pentium IV Processor of 2.80 GHz, and RAM of 2.5 GB. From Table 1., it is seen that the computational efficiency of the sectional model is around 150% higher than of the fiber model.

4.2 Dynamic analysis

The structure, as shown in Fig. 10 (a), is a four-story steel frame with three spans in the long direction and two spans in the short direction. The plane frame at the axis 2 is chosen for dynamic analysis subjected to earthquake. The information on dimension, section type, member numbering and vertical load numbering of the frame is shown in Fig. 10 (b); the dimension of different section is listed in Table 2.

The lumped masses on exterior and interior columns at the roof are 5 t and 10 t, respectively; they are 10 t and 20 t at the other floors. To reflect the effects of axial force more significantly, the vertical load induced by the weight of the structure is increased two times as normal. Hence, the vertical loads on the beam-column joints are $P_{1/2/3}^{ex}$ = 200 kN and P_4^{ex} = 100 kN for exterior columns, and $P_{1/2/3}^{in}$ = 400 kN and P_4^{in} = 200 kN for interior columns. The Rayleigh damping matrix is determined based on a damping ratio of 0.02 for the first two modes of the structure. In this analysis, plasticity is assumed only on the columns and their modeling is the same as in the last subsection, while the beams are represented with elastic beam elements.

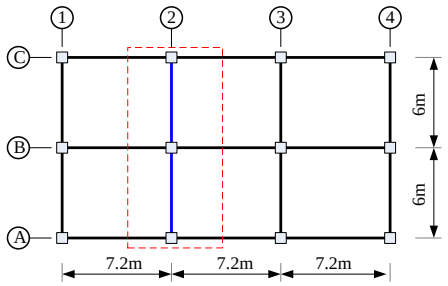

(a) Planform of the prototype steel frame

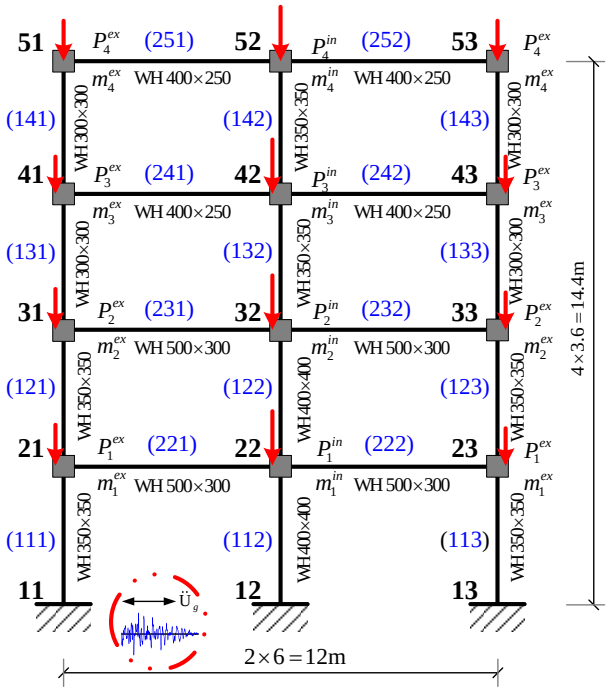

(b) Dimensions and loads of the plane frame

Figure 10. Plane steel frame structure to be studied.

Table 2. The section dimension and features of welded steel H-section

Member type	Section type	dimensions (mm)				Area (A) (cm^2)	Moment of area (I_z) (cm^4)
		d	b_f	t_w	t_f		
Column	WH 400×400	400	400	8	14	142.0	45170
	WH 350×350	350	350	8	12	110.0	26310
	WH 300×300	300	300	8	12	94.1	16340
Beam	WH 500×300	450	300	8	16	133.0	63080
	WH 400×250	400	250	8	12	90.1	26130

The earthquake record El Centro (NS 1940) is used as horizontal excitation with peak ground acceleration of 310 cm/s^2. The α-Operator splitting [26] algorithm is employed for time integration, and integration interval is 0.02 s.

In Fig. 11, the global response are compared among the there models. The time history of roof horizontal displacement in section model is very close to that in fiber model as shown in Fig. 11 (a). Besides, the max inter-story drift angle of each floor in sectional model approximates to that in fiber model as shown in Fig. 11 (b). All these illustrate that the proposed sectional constitutive law is acceptable in computational accuracy. In contrast, the errors with plastic hinge are easily observed, although it basically agrees with the fiber model.

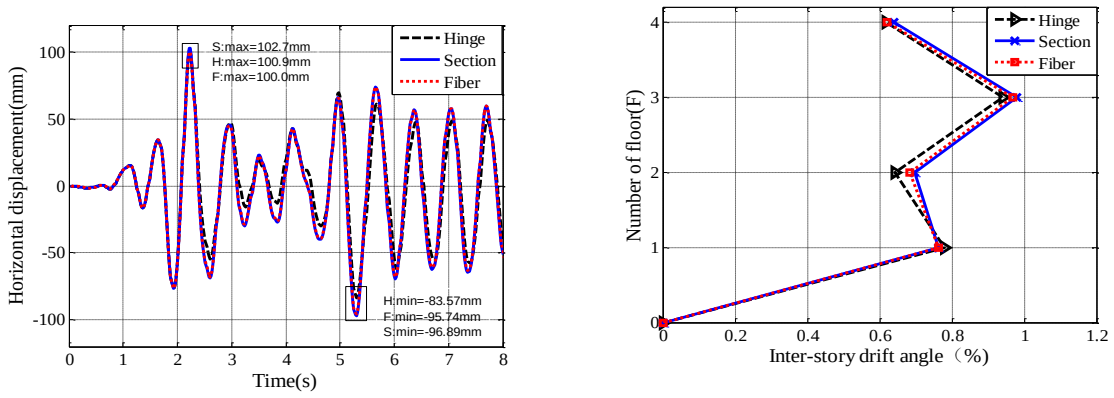

(a) Time history of roof horizontal displacement *(b) Max inter-story drift angle of each floor*

Figure 11. Global response of the frame structure.

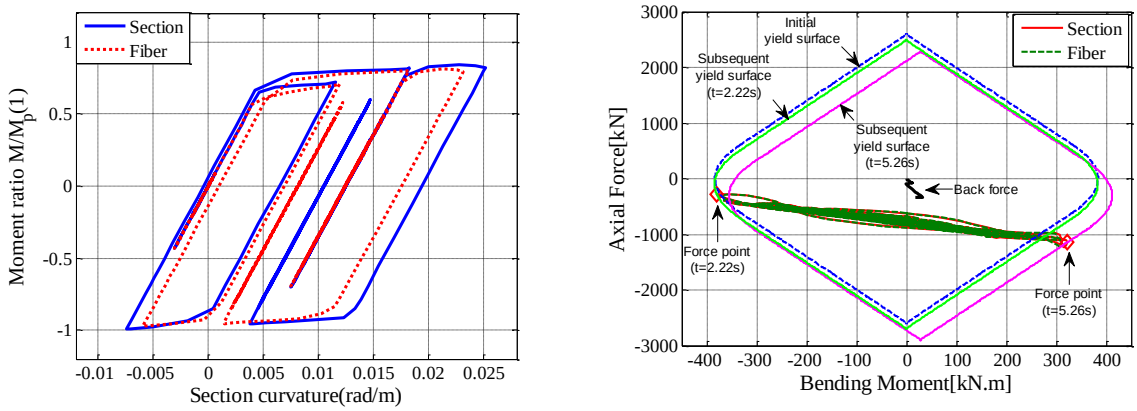

(a) Moment ratio vs. section curvature *(b) Force path and section NM yield surface*

Figure 12. Local response of column 111 at bottom section.

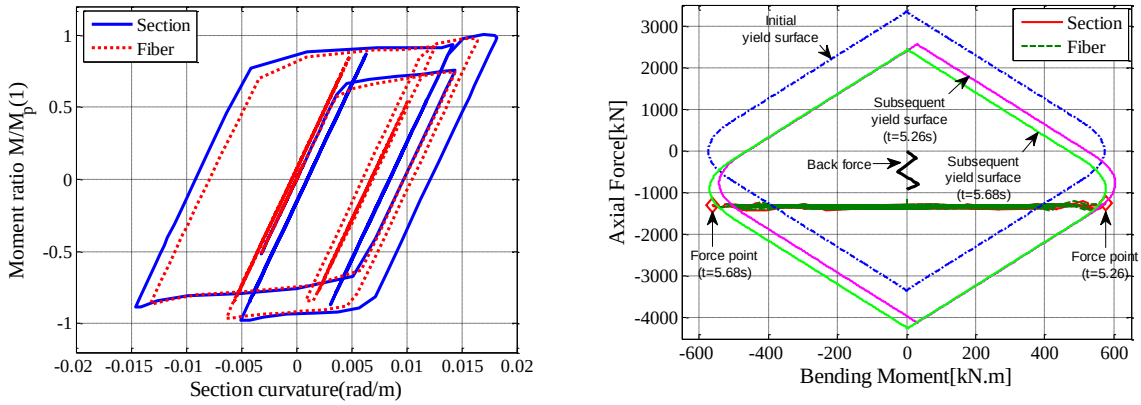

(a) Moment ratio vs. section curvature *(b) Force path and section NM yield surface*

Figure 13. Local response comparison at bottom section of column 112.

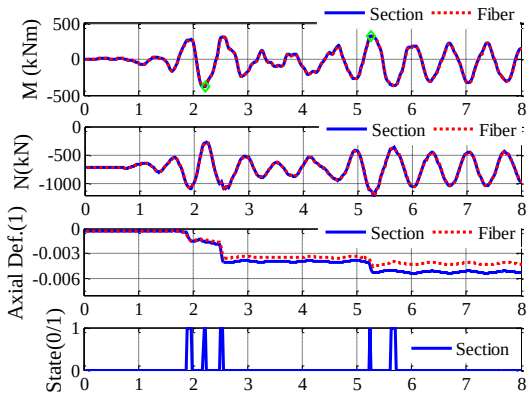

(a) Bottom section of column 111

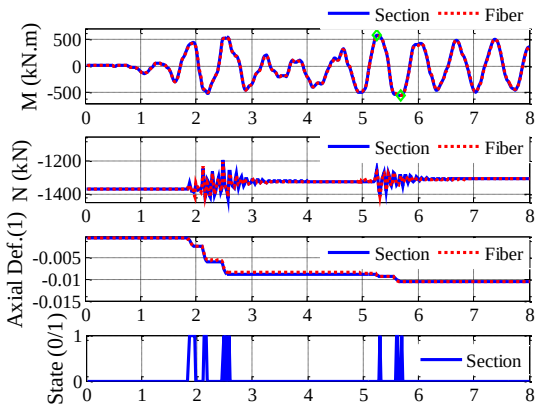

(b) Bottom section of column 112

Figure 14. Time history of force/deformation and section state at the bottom section.

Figures 12-14 show the local responses of Columns 111 and 112 at the bottom section. The moment-curvature responses are shown in Figures 12 (a) and 13 (a), where it is seen that, although the local responses with the two approaches do not agree so well as the global responses, the error of the sectional model appears acceptable. Figures 12 b and 13 (b) show the internal force paths and yield surfaces. Two subsequent yield surfaces for each column are plotted so as to correspond to the positive and negative maximum bending moments. From Figures 12 (b) and 13 (b), it is seen that the axial force of the middle column keeps nearly constant while that of side column varies from about 300 kN to 1200 kN, which reflects the additional axial force onto the side column caused by overturning.

Fig. 14 compares the time histories of section forces and axial deformation of the two models and also gives the section state of the sectional model. It is clearly seen that the responses of the sectional model agrees quite well with those of the fiber model in the presence of variable axial force. From the time history of state indicator with the sectional model, we see that the section enters plastic state when the axial deformation is relatively significantly increased. In addition, the axial force of the middle column becomes oscillatory as the section switches between plastic and elastic states. These phenomena are confirmed by the analysis with fiber model using OpenSEES as shown in Fig. 14.

The time consumption of dynamic analysis with the two models both written in MATLAB is also recorded. The computation environment is the same as that in the last subsection. The computational time for the sectional model is 20.76 s, while the fiber model is 65.48 s; the efficiency of the former is about two times higher than the latter.

5 Conclusion

A novel sectional constitutive model with mixed-hardening is proposed for beam-column element in the framework of classical plasticity theory. The sectional model features kinematic/isotropic-hardening. It can account for axial force and bending moment coupling, and can be used for distributed plasticity beam-column models. The model is validated by numerical examples of static cyclic analysis of a cantilever column and dynamic analysis of a steel frame structure. The numerical results show that the proposed sectional model has higher accuracy than a plastic hinge model and higher computational efficiency than a fiber model.

Acknowledgements

This research paper is based upon work supported by the National Natural Science Foundation of China under Grants No. 51161120360 and No. 91315301-09, and the authors gratefully acknowledge these supports.

References

[1] Spacone, E., Ciampi, V., Filippou, F. C.: *Mixed formulation of nonlinear beam finite element,*

Computers & Structures, 58 (1996), 1, pp. 71-83.

[2] Ibarra, L.F., Medina, R. A., Krawinkler, H.: *Hysteretic models that incorporate strength and stiffness deterioration*. Earthquake Engineering & Structural Dynamics, 34 (2005), 12, pp. 1489–1511.

[3] Mander, J.B., Priestley, M.J.N., Park, R.: *Theoretical stress-strain model for confined concrete*, Journal of structural Engineering, ASCE, 114 (1988), ST8, pp. 1804-1826.

[4] Kwak, H.G., Kim, S.P.: *Nonlinear analysis of RC beams based on moment-curvature relation*, Computers & Structures, 80 (2002), pp. 615-628.

[5] Kwak, H.G., Kim, S.P.: *Simplified monotonic moment-curvature relation considering fixed-end rotation and axial force effect*, Engineering Structures, 32 (2010), pp. 69-79.

[6] Vaz, M.A., Patel, M.H.: *Post-buckling behavior of slender structures with a bi-linear bending moment-curvature relationship*, International Journal of Non-Linear Mechanics, 42 (2007), pp. 470-483.

[7] Morris, G.A., Fenves, S.J.: *Elastic-plastic analysis of frameworks*, Journal of the Structural Division, 96 (1970), 5, pp. 931-946.

[8] Nigam, N.C.: *Yielding in framed structures under dynamic loads*, Journal of the Engineering Mechanics Division, 96 (1970), 5, pp. 687-709.

[9] Wen, R.K., Farhoomand, F.: *Dynamic analysis of inelastic space frames*, Journal of the Engineering Mechanics Division, 96 (1970), 5, pp. 667-686.

[10] Orbison, J.G., William, M.G., John, A.F.: *Yield Surface application in nonlinear steel frame analysis*, Computer Methods in Applied Mechanics and Engineering, 33 (1982), pp. 557-573.

[11] Powell, G.H., Chen, P.F.S.: *3D Beam-Column Element with Generalized Plastic Hinges*, Journal of Engineering Mechanics, 112 (1986), 7, pp. 627-641.

[12] White, D.W.: *Plastic-hinge methods for advanced analysis of steel frames*, Journal of Construction Steel Research, 24 (1993), 2, pp. 121-52.

[13] Shu, X.P., Shen, P.S.: *Geometrical and Material Nonlinear Analysis of The Ultimate Strength of Steel frames*, Chinese Journal of Engineering Mechanics, 10 (1993), 4, pp. 32-41 (in Chinese).

[14] Chan, S.L., Chui, P.T.: *A generalized design-based elasto-plastic analysis of steel frames by section assemblage concept*, Engineering. Structures, 19 (1997), 8, pp. 628-636.

[15] Iu, C.K., Bradford, M.A., Chen, W.F.: *Second-order inelastic analysis of composite framed structures based on the refined plastic hinge method*, Engineering Structures, 31 (2009), 3, pp. 799-813.

[16] Biglari, A., Harrison, P., Bićanić, N.: *Quasi-hinge beam element implemented within the hybrid force-based method*, Computers & Structures, 137 (2014), 6, pp. 31-46.

[17] Roncevic, B., Turkalj, G.: *Application of plastic hinges in finite element analysis of framed structures*, Engineering Review, 26 (2006), pp. 75-87.

[18] Baptista, A.M.: *Resistance of steel I-sections under axial force and biaxial bendin*, Journal of Constructional Steel Research, 72 (2012), pp. 1-11.

[19] Hosseini, M., Abbas, H.: *Strain hardening in M-P interaction for metallic beam of I-sectio*, Thin-Walled Structures, 62 (2013), pp. 243-256.

[20] Chen, W.F. et al.: *Elasticity and plasticity*. Architecture & Building Press, Beijing, China, 2005.

[21] Simo, J.C., Taylor, R.L.: *Return mapping algorithm for plane stress elastoplasticity*, International Journal for Numerical Methods in Engineering, 22(1986), pp. 649-670.

[22] Bhatti, M.A.: *Advanced Topics in Finite Element Analysis of Structures: with Mathematica and Matlab computations*. John Wiley &Sons, New York, 2006.

[23] National Development and Reform Commission, *PRC: The Weld Steel H-Section. Standards for Ferrous Metallurgy Industry*, YB 3300-2005, v3 (2005), pp. 2-7.

[24] Mathworks, MATLAB, *the language of technical computing*, 2009.

[25] McKenna, F., Fenves, G.L., Scott, M.H.: *Open system for earthquake engineering simulation*, University of California, Berkeley, CA (2000), online: http://opensees.berkeley.edu/.

[26] Combescure, D., Pegon, P.: *α-Operator splitting time integration technique for pseudo dynamic testing error propagation analysis*, Soil Dynamic and Earthquake Engineering, 16 (1997), pp. 427-443.